Z. Physik A - Atoms and Nuclei 295, 37-43 (1980)

Zeitschrift für Physik A Atoms and Nuclei

Doppler-Free Two-Photon Laser Spectroscopy of Barium I: Hyperfine Splitting and Isotope Shift of High Lying Levels

W. Jitschin* and G. Meisel
Institut für Angewandte Physik der Universität Bonn, Bonn, Fed. Rep. Germany

Received December 21, 1979

The Doppler-free two-photon absorption method performed with a narrowband *cw* dye laser permitted high resolution measurements of transitions from the Ba I ground state $6s^2\,{}^1S_0$ to several highly excited states. The lifetimes and hyperfine splittings of these states as well as the isotope shifts of the transitions have been determined accurately. The lifetime values are in agreement with transition probability data; the hyperfine splitting results show considerable configuration interaction effects. A detailed discussion of the isotope shifts is given.

1. Introduction

The atomic spectrum of barium has been the subject of several investigations in the past. On the one hand the interest has focused on the identification of energy levels, and even recently new term assignments were obtained [1, 2]. On the other hand from the hyperfine structure of the levels information on electromagnetic moments and spins of the atomic nuclei can be deduced. Natural barium essentially consists of 5 stable isotopes, but more than 20 isotopes have lifetimes longer than 1 s. Investigations of the hyperfine structure have been done on Ba I [3-6] as well as on Ba II [7-10]. The stable isotope with largest mass, ^{138}Ba, has magic neutron number 82 which results in a comparatively small nuclear size. The nuclear charge radii for a large number of stable and unstable isotopes have also been the subject of recent isotope shift investigations [5].

In contrast to the Ba fine structure, the understanding of the hyperfine structure is not yet satisfactory [11]. It is known only for a few low-lying energy levels with moderate accuracy. The aim of this work was to determine the hyperfine structure of a larger number of levels with high accuracy. For this purpose we applied the Doppler-free two-photon method [12-14] which allowed us to reach several high-lying levels using visible laser light. The use of two counter-propagating laser beams eliminates the first order Doppler-effect and therefore permitted us to obtain the high resolution corresponding to the natural width of the transitions without the necessity of any collimation of the atomic beam.

2. Experimental

A scheme of the experimental setup is shown in Fig. 1. The barium is evaporated from an oven at temperatures between 590 K and 820 K. The oven is heated by a Ta foil of 15 μm thickness with currents of 30 to 45 A. The heater arrangement is bifilar to keep magnetic stray fields caused by the heater current below 10^{-4} T in the neighbouring interaction region. In the interaction zone the barium atomic beam is crossed by two counter-propagating laser beams. If a barium atom undergoes a two-photon absorption process, it can decay from the excited state via several decay channels. For the detection of the resonances the ultraviolet decay photons were used since they could be well discriminated against laser and oven stray light by a color glass filter (Oriel type G-774-4000). The fluorescence light to be detected leaves the vacuum chamber through a fused silica window which is heated to about 570 K to prevent

* Now at Fakultät für Physik, Universität Bielefeld, D-4800 Bielefeld 1, Fed. Rep. Germany

0340-2193/80/0295/0037/$01.40

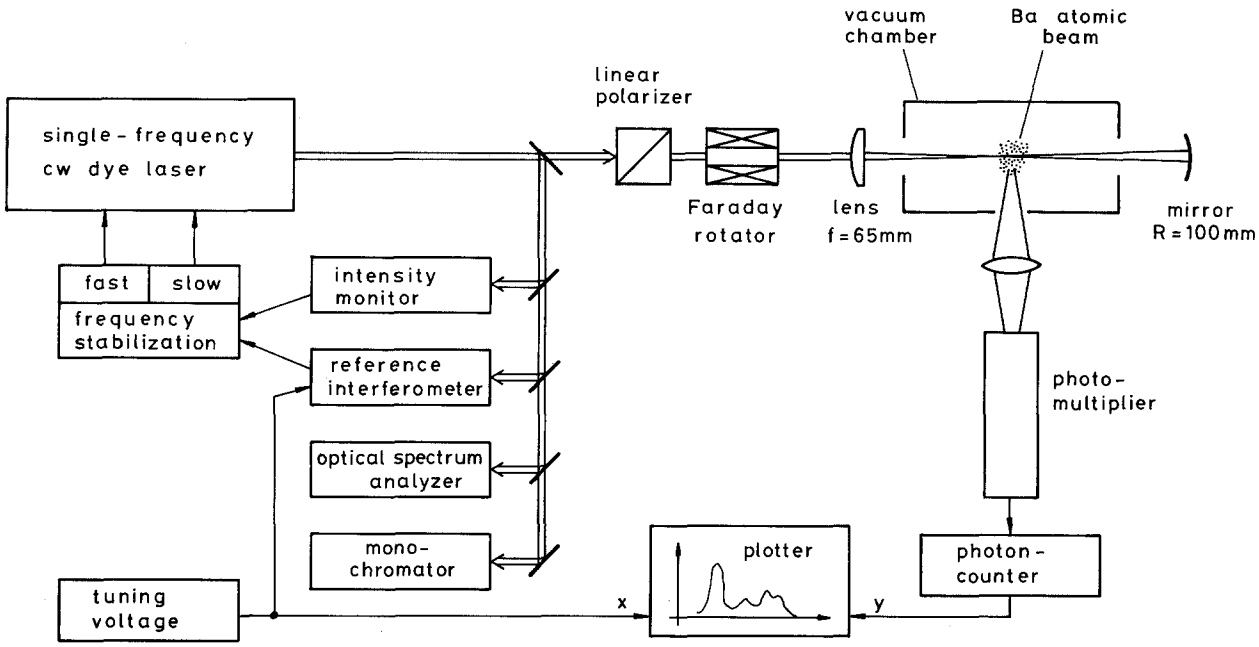

Fig. 1. Schematic diagram of the experimental setup

deposition of Ba metal. The light is collected from a solid angle of $0.03 \cdot 4\pi$ by a fused silica lens and focused onto a bialkali photomultiplier with low dark current (type 9635B by EMI). To improve the signal-to-noise ratio the photomultiplier was cooled and photon counting techniques were employed. Typical count rates were $10^4\,s^{-1}$ with the laser tuned to the peak of the strongest resonance line and $20\,s^{-1}$ without laser light.

The laser system used in our experiment was a commercial *cw* dye laser (model 580 A by Spectra-Physics). To obtain single frequency output power of up to 200 mW several dispersive elements including an additional uncoated etalon of 30 μm thickness were inserted into the laser cavity. The frequency stability of the free-running laser was too poor for high resolution measurements; therefore a frequency stabilization system was built. For this purpose a small part of the laser output was sent through a confocal reference interferometer (Spectra-Physics model 450-03). The slope at half height of a transmission peak was used as laser frequency discriminator. A frequency deviation was identified as a change of the transmitted intensity; the error signal obtained was split by a frequency dividing network into its fast and slow components and fed to two piezoelectric mirror translators. One of them allowed large but slow motions whereas the other one was built for high response speed in order to obtain a fast servo system. Thus fast laser frequency deviations could also be compensated resulting in a small laser bandwidth of less than 1 MHz *rms*.

The main output beam of the laser was sent to the atomic beam apparatus where it was focused to 20 μm diameter in the interaction region by a lens with 65 mm focal length. It was then focused back into itself by a spherical mirror to obtain the counter-propagating light beam. In order to protect the laser against the returning beam a linear polarizer and a 45° Faraday polarization rotator were used as light trap.

The laser frequency was tuned by changing the length of the reference interferometer piezoelectrically. The voltage applied to the spacers was taken for the horizontal deflection of an *x*-*y*-plotter which recorded the resonance spectra. The calibration of the horizontal frequency axis was performed by means of a HeNe laser which emitted light in two longitudinal modes. The frequency difference of the modes was accurately determined by optical heterodyning methods and the frequency spectrum of the laser was recorded via the reference interferometer using it as an optical spectrum analyzer. Thus the interferometer's voltage-to-frequency calibration at the HeNe laser wavelength was obtained. This calibration can be transferred to other wavelengths by multiplication by the wavelength ratio. The uncertainty of this calibration results mainly from technical problems: The length changes of the piezoelectric spacers in the interferometer do not depend linearly on the electrical voltage, there is hysteresis and also considerable drift due to ambient temperature and pressure changes. Furthermore the piezoelectric sensitivity depends on the temperature. In order to compensate for these

effects in the experiment, all spectra were recorded about 40 times by tuning the laser frequency up and down at constant speed. The final frequency values were obtained as averages of these runs. In cases where a transition line splits into several resolved hyperfine components, consistency checks were performed taking into account the splittings and shifts due to magnetic dipole and electric quadrupole interactions [15]. It was found that the final values exhibit consistency within an accuracy of $\pm 0.4\%$. The absolute accuracy of the calibration covering also the ambient temperature changes is estimated to be about $\pm 1.5\%$.

Since in a two-photon transition the change of atomic energy is twice the photon energy, the frequency difference of atomic lines is just two times the laser frequency detuning. To avoid confusions all atomic frequency values given in this paper are related to the atomic system.

3. Results

In all measurements the initial atomic state was the Ba I ground state $6s^2\,{}^1S_0$. By two-photon absorption excited states with $J'=0$ or $J'=2$ and with the same parity as the ground state can be populated; this is complementary to single photon absorption where odd parity states with $J'=1$ are accessible from the Ba I ground state. The transitions to excited states as listed in Table 1 were observed and analyzed. The energy values and level designations were taken from [16] with corrections according to recent results [1, 2] which were confirmed by our work.

We have used natural barium for our experiment; the resonance lines obtained belong to the most abundant isotopes ^{138}Ba (71.7%), ^{137}Ba (11.3%), ^{136}Ba (7.8%), ^{135}Ba (6.6%) and ^{134}Ba (2.4%). For transitions to $J'=0$ excited states five unsplit resonances corresponding to the five isotopes are expected. It is to be noted that also for the odd isotopes no hyperfine splitting is present for the $J=0\rightarrow J'=0$ transitions. For transitions to $J'=2$ states the lines corresponding to the odd isotopes ^{137}Ba ($I=3/2$) and ^{135}Ba ($I=3/2$) each split into four hyperfine components for $F'=7/2$, 5/2, 3/2 and 1/2, so that altogether eleven lines are expected in these cases. In most spectra not all lines can be resolved due to the natural linewidth. Figures 2 and 3 show two relatively well resolved transitions to $J'=0$ and $J'=2$ states.

In order to analyze the spectra the hyperfine splitting of the two odd isotopes was considered first. The relative position of a single hyperfine component with respect to the center of gravity was described by the two parameters A and B for the nuclear magnetic dipole and electric quadrupole interaction [15]. The factors A and B depend on the transition and the isotope considered. Their ratio for different isotopes, however, is the same for all transitions except for small corrections which can be ignored within the accuracy of the present data. The ratio was therefore taken from precision rf measurements [17]:

$$A(^{137}\mathrm{Ba})/A(^{135}\mathrm{Ba})=1.119$$
$$B(^{137}\mathrm{Ba})/B(^{135}\mathrm{Ba})=1.54.$$

Using these ratios the splitting of the eight hyperfine components corresponding to the two odd barium

Table 1. Ba I two-photon resonances investigated in this work and their observed experimental linewidths. For the designation of the upper levels see text

Upper level energy [cm^{-1}]	Laser wavelength [Å]	Exp. linewidth (FWHM) [MHz]	Transition
34,493.898	5,796.520	31 (3)	$6s^2\,{}^1S_0\rightarrow 6p^2\,{}^3P_0$
35,616.947	5,613.746	22 (2)	$\rightarrow 6p^2\,{}^3P_2$
34,370.984	5,817.249	19 (3)	$\rightarrow 6s8s\,{}^1S_0$
37,234.185	5,369.915	6 (1)	$\rightarrow 6s9s\,{}^1S_0$
35,344.423	5,657.032	27 (2)	$\rightarrow 6s7d\,{}^1D_2$
35,762.211	5,590.943	14 (2)	$\rightarrow 6s7d\,{}^3D_2$
37,434.956	5,341.114	12 (1)	$\rightarrow 6s8d\,{}^1D_2$
33,795.840	5,916.249	18 (2)	$\rightarrow 5d7s\,{}^1D_2$
36,200.423	5,523.263	19 (2)	$\rightarrow 5d6d\,{}^3D_2$

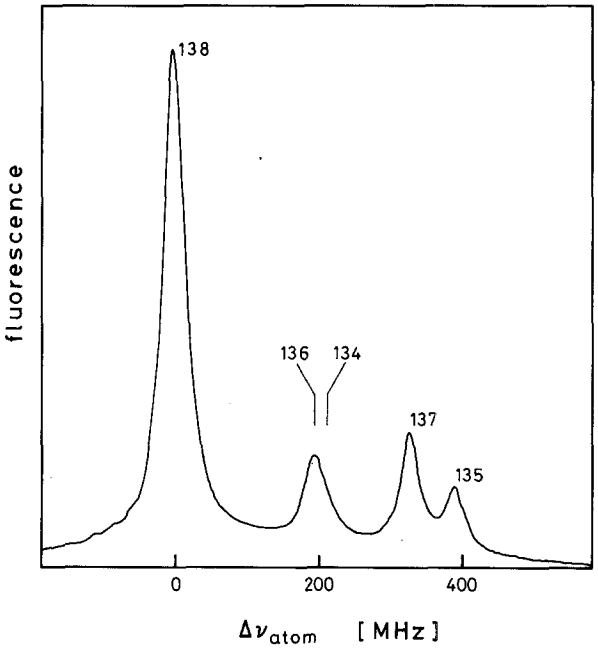

Fig. 2. Record of the two-photon transition $6s^2\,{}^1S_0\rightarrow 6p^2\,{}^3P_0$ of Ba with line identification by isotope mass number

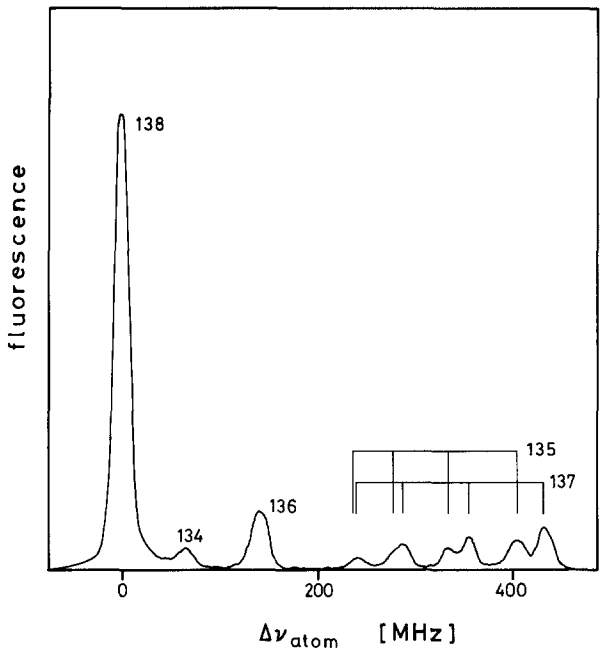

Fig. 3. Record of the two-photon transition $6s^2\,{}^1S_0 \rightarrow 5d6d\,{}^3D_2$ of Ba with line identification by isotope mass number

Table 2. Hyperfine splitting factors of the $J'=2$ states for ^{137}Ba.

Level	$A(^{137}\mathrm{Ba})$ [MHz]	$B(^{137}\mathrm{Ba})$ [MHz]
$6p^2\,{}^3P_2$	+333.0 (5.0)	−22.7 (7.3)
$6s7d\,{}^1D_2$	+ 69.1 (1.0)	−30.1 (3.6)
$6s7d\,{}^3D_2$	+ 38.2 (0.6)	+ 4.7 (3.3)
$6s8d\,{}^1D_2$	+ 41.6 (0.7)	+32.3 (3.7)
$5d7s\,{}^1D_2$	−115.2 (1.7)	+41.3 (8.2)
$5d6d\,{}^3D_2$	+ 24.6 (0.9)	−15.1 (5.8)

isotopes can be described with only two free parameters; thus the interpretation of spectra with unresolved lines was considerably facilitated. A computer fit yielded the two parameters $A(^{137}\mathrm{Ba})$ and $B(^{137}\mathrm{Ba})$ as well as the centers of gravity for the two isotopes. The results for the hyperfine splitting factors are shown in Table 2.

In order to determine the isotope shifts, the frequency scale was arbitrarily set to zero at the strong line corresponding to ^{138}Ba. The obtained isotope shift values are given in Table 3.

4. Discussion

4.1. Lifetimes

Direct information obtained from the measurements is the width of the resonance line (see Table 1). The observed width is a convolution of the natural linewidth and of the experimentally induced broadening (laser jitter, transit-time broadening, Zeeman-broadening in case of $J' \neq 0$ states, etc.). The smallest width observed was 6 MHz so that the instrumental contribution to the width cannot be greater than 6 MHz, in good agreement with estimates of the experimental broadening effects. Since the linewidths in all other transitions are larger, it is concluded that they are mainly determined by the natural width. From the natural width $\Delta\nu$ the lifetime τ of the excited state can be obtained according to $\tau = 1/(2\pi \cdot \Delta\nu)$. The lifetime values calculated from our data are in good agreement with values estimated from experimental transition probabilities [18].

4.2. Hyperfine Splittings

The hyperfine splittings have been measured for six levels belonging to different configurations. Since Ba I has two outer electrons, the hyperfine splitting can theoretically be analyzed by considering the independent interaction of each of the two electrons with the nuclear moments and taking the electron-electron interaction via angular momentum algebra into ac-

Table 3. Measured isotope shift values. The shift is defined as $\nu(^{138}\mathrm{Ba}) - \nu(^{A}\mathrm{Ba})$, see e.g. [24]. A dash indicates an unresolved line

Transition	^{138}Ba [MHz]	^{137}Ba [MHz]	^{136}Ba [MHz]	^{135}Ba [MHz]	^{134}Ba [MHz]
$6s^2\,{}^1S_0 \rightarrow 6p^2\,{}^3P_0$	0	−331.7 (5.0)	−199.0 (3.0)	−396.1 (5.9)	−219.0 (9.9)
$\rightarrow 6p^2\,{}^3P_2$	0	−220.4 (4.4)	−114.9 (4.1)	−243.5 (7.2)	–
$\rightarrow 6s8s\,{}^1S_0$	0	−159.5 (2.4)	− 77.7 (1.4)	−167.4 (3.2)	− 64.9 (6.1)
$\rightarrow 6s9s\,{}^1S_0$	0	−107.6 (2.0)	− 35.8 (1.0)	− 92.4 (2.0)	–
$\rightarrow 6s7d\,{}^1D_2$	0	−321.5 (4.8)	−183.8 (4.1)	−369.1 (5.5)	–
$\rightarrow 6s7d\,{}^3D_2$	0	−126.9 (1.9)	− 51.0 (2.0)	−121.7 (1.8)	–
$\rightarrow 6s8d\,{}^1D_2$	0	−188.7 (2.8)	− 92.9 (3.0)	−200.8 (3.0)	− 75.9 (3.0)
$\rightarrow 5d7s\,{}^1D_2$	0	−306.4 (5.2)	−119.7 (2.0)	−286.0 (5.1)	− 49.7 (2.0)
$\rightarrow 5d6d\,{}^3D_2$	0	−365.3 (5.5)	−146.2 (2.2)	−346.4 (5.2)	− 65.9 (3.0)

count. In particular, the ratios of A or B factors of certain levels within a configuration are independent of the nuclear moments and can therefore be calculated by angular momentum algebra, the results depending on the angular momentum coupling assumed. It was found, however, that neither LS- or jj-coupling nor intermediate coupling reproduced the experimental ratios; there were strong discrepancies both in magnitude and sign. These discrepancies could not be overcome by application of a more elaborate theory using effective radial parameters [19]. This indicates that strong configuration interaction in the investigated levels is present. Considerable configuration interaction can also be deduced from the experimental fine structure intervals, from multichannel quantum-defect analysis of experimental data [2] as well as from theoretical calculations [e.g. 20, 21].

4.3. Isotope Shifts

The isotope shift $\Delta\nu_i^{AA'}$ between two isotopes with mass numbers A and A' in a spectral line i results from two effects: Firstly from the change of nuclear mass (mass shift) and secondly from the change of size and shape of the nuclear charge distribution (field shift). The isotope shift is the sum of both effects [11, 22]:

$$\Delta\nu_i^{AA'} = M_i \cdot \frac{A'-A}{AA'} + F_i \cdot \delta\langle r^2\rangle^{AA'}, \tag{1}$$

where M_i and F_i are electronic factors which are characteristic for the transition and $\delta\langle r^2\rangle$ takes into account the size and shape of different nuclei. The mass effect again is the sum of two contributions; one is the so-called normal mass shift which is easily calculated to be $\nu_i \cdot (m_e/m_p) \cdot (A'-A)/AA'$, where ν_i is the optical transition frequency and m_e/m_p is the electron-to-proton mass ratio. The second contribution is called specific mass shift which in most cases is not easily determined.

Equation (1) can be rewritten introducing the so-called modified isotope shift $\zeta_i^{AA'}$ [11]:

$$\zeta_i^{AA'} := \Delta\nu_i^{AA'} \cdot \frac{AA'}{A'-A} = M_i + F_i \cdot \frac{AA'}{A'-A}\delta\langle r^2\rangle^{AA'}. \tag{2}$$

The consistency of isotope shift measurements with ansatz (1) can be checked by comparing the modified isotope shifts for two different transitions i and j; it follows from (2) that

Table 4. Change of total electron density at the nucleus for two-photon transitions i. Values are normalized to the electron density change in the $6s^2\,{}^1S_0 \rightarrow 6s6p\,{}^1P_1^o$ one-photon transition j, whose data have been taken from [5]

Transition i	$\frac{\Delta\lvert\Psi(0)\rvert_i^2}{\Delta\lvert\Psi(0)\rvert_j^2}$
$6s^2\,{}^1S_0 \rightarrow 6s6p\,{}^1P_1^o$	1
$\rightarrow 6p^2\,{}^3P_0$	1.538 (30)
$\rightarrow 6p^2\,{}^3P_2$	1.082 (32)
$\rightarrow 6s8s\,{}^1S_0$	0.796 (15)
$\rightarrow 6s9s\,{}^1S_0$	0.594 (13)
$\rightarrow 6s7d\,{}^1D_2$	1.525 (35)
$\rightarrow 6s7d\,{}^3D_2$	0.673 (14)
$\rightarrow 6s8d\,{}^1D_2$	0.942 (14)
$\rightarrow 5d7s\,{}^1D_2$	1.626 (20)
$\rightarrow 5d6d\,{}^3D_2$	1.936 (23)

$$\zeta_i^{AA'} = \left(M_i - M_j\frac{F_i}{F_j}\right) + \frac{F_i}{F_j}\cdot\zeta_j^{AA'}, \tag{3}$$

i.e. there should be a linear relationship between ζ_i and ζ_j. The modified isotope shifts for different isotope pairs A, A' should lie on a straight line with slope F_i/F_j and intercept $M_i - M_j F_i/F_j$ in a King plot [23].

We have determined the best fitting straight lines through our data points. Furthermore we included isotope shift data for the Ba resonance transition $6s^2\,{}^1S_0 \rightarrow 6s6p\,{}^1P_1^o$ as given in [5] and [6]. The experimental data of both works fairly agree; in our calculations the data from [5] were used because their quoted errors are smaller. From all fits it was found that the straight King lines well describe the experimental data points within the experimental errors. The slope F_i/F_j of a line is a purely electronic quantity, where F is proportional to $\Delta|\Psi(0)|^2$, the change of the total electron density at the nucleus. Therefore from the experimental F_i/F_j values the ratios $\Delta|\Psi(0)|_i^2/\Delta|\Psi(0)|_j^2$ can be determined. In order to compare the results, for j the fixed single photon transition $6s^2\,{}^1S_0 \rightarrow 6s6p\,{}^1P_1^o$ was chosen; the results are given in Table 4. As can be seen, $\Delta|\Psi(0)|_i^2$ varies considerably; since the lower state is the same for all transitions the variation is due to a change of $|\Psi(0)|^2$ of the upper states. Particularly the electron density at the nucleus is not constant within different levels of a term that nominally belong to the same configuration, e.g. $6p^2\,{}^3P_0$ and ${}^3P_2$. This indicates strong second order mixing effects in the upper states.

From the intercept values of the fitted straight lines a relation between the mass and field effects is obtained. In order to separate both effects additional information is required. It is known that in

Table 5. Separated mass- and field-shift data. The data for the $6s^2\,{}^1S_0 \rightarrow 6s6p\,{}^1P_1^o$ transition have been taken from [5]

Transition	Specific mass shift for $\Delta A=1$		Field shift			
	absolute [MHz]	as fraction of normal mass shift	$\Delta\nu^{137,138}$ [MHz]	$\Delta\nu^{136,138}$ [MHz]	$\Delta\nu^{135,138}$ [MHz]	$\Delta\nu^{134,138}$ [MHz]
$6s^2\,{}^1S_0 \rightarrow 6s6p\,{}^1P_1^o$	0 (8)	0.0 (5)	−231 (8)	−160 (16)	−308 (24)	−207 (32)
$\rightarrow 6p^2\,{}^3P_0$	− 5 (12)	−0.2 (4)	−355 (12)	−247 (25)	−474 (37)	−318 (50)
$\rightarrow 6p^2\,{}^3P_2$	− 1 (9)	0.0 (3)	−250 (9)	−173 (18)	−334 (28)	–
$\rightarrow 6s8s\,{}^1S_0$	− 5 (6)	−0.2 (2)	−184 (6)	−128 (13)	−246 (19)	−165 (26)
$\rightarrow 6s9s\,{}^1S_0$	− 3 (5)	−0.1 (1)	−137 (5)	− 95 (10)	−183 (15)	–
$\rightarrow 6s7d\,{}^1D_2$	+ 1 (12)	0.0 (4)	−352 (12)	−245 (25)	−470 (38)	–
$\rightarrow 6s7d\,{}^3D_2$	− 3 (5)	−0.1 (2)	−155 (5)	−108 (11)	−207 (17)	–
$\rightarrow 6s8d\,{}^1D_2$	− 3 (7)	−0.1 (2)	−217 (7)	−151 (15)	−291 (23)	−195 (30)
$\rightarrow 5d7s\,{}^1D_2$	+41 (13)	+1.4 (4)	−375 (13)	−261 (26)	−502 (39)	−336 (52)
$\rightarrow 5d6d\,{}^3D_2$	+51 (15)	+1.6 (5)	−446 (15)	−310 (31)	−597 (46)	−400 (62)

$ns^2 \rightarrow nsnp$ transitions the specific mass effect can be estimated to be 0 ± 0.5 times the normal mass effect [11]; this yields a total mass effect for the transition $6s^2\,{}^1S_0 \rightarrow 6s6p\,{}^1P_1^o$ of (15.6 ± 7.8) MHz. A critical discussion of the mass effect in this line can be found in [6]. Using the number given the mass effect as well as the field effect in the two-photon transitions have been determined. From the mass shift values obtained the normal mass shift (29 to 32 MHz depending on the transition) has been subtracted leading to the specific mass shift values. The results are given in Table 5. It can be seen that the specific mass shift is almost zero in most transitions, but it is significantly different from zero in transitions to final states with one $5d$ electron. A different approach to separate mass and field effects is the application of the bunching method [24]. It was found that this method gives the same separation into both effects within the uncertainty caused by the errors of the experimental data [25].

The King plot is a form of the ansatz (1) with the nuclear parameters eliminated. The electronic parameters also can be eliminated. There are several ways to do so and we have chosen the following combinations:

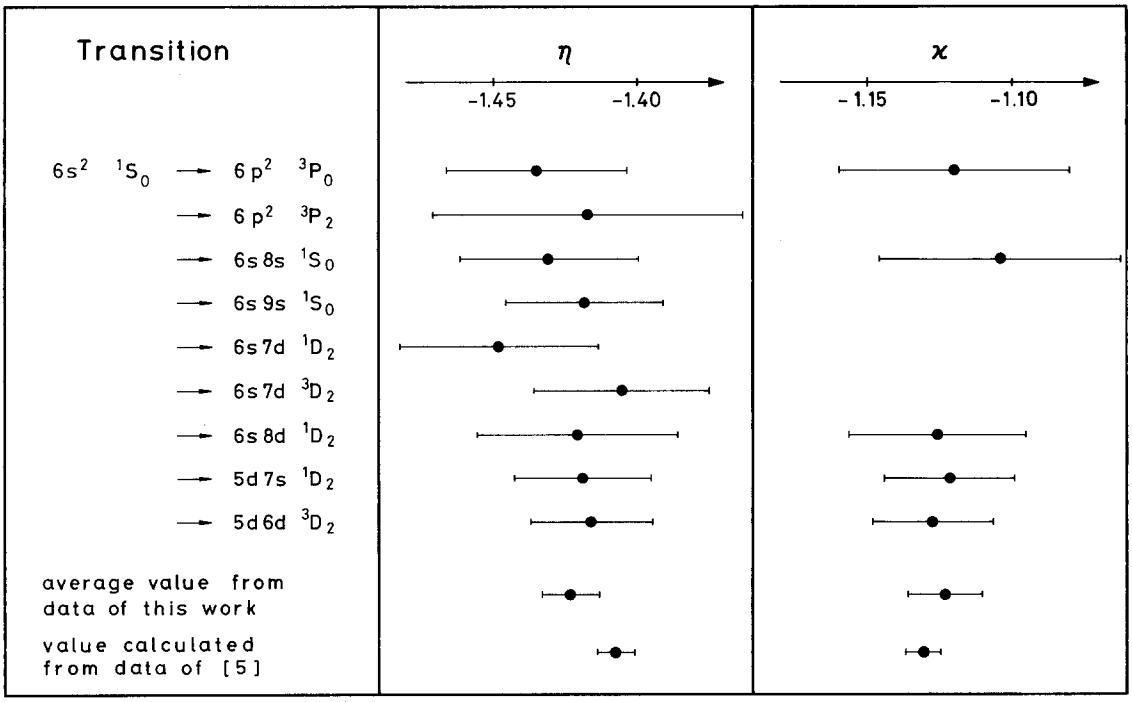

Fig. 4. Nuclear parameters η and κ (as defined by equations (4) and (5)) calculated from different electronic transitions

$$\eta_i := \frac{\zeta_i^{136,137} - \zeta_i^{137,138}}{\zeta_i^{135,136} - \zeta_i^{136,137}} = \frac{137}{136} \cdot \frac{136 \cdot \delta\langle r^2\rangle^{136,137} - 138 \cdot \delta\langle r^2\rangle^{137,138}}{135 \cdot \delta\langle r^2\rangle^{135,136} - 137 \cdot \delta\langle r^2\rangle^{136,137}} \quad (4)$$

$$\kappa_i := \frac{\zeta_i^{134,135} - \zeta_i^{135,136}}{\zeta_i^{135,136} - \zeta_i^{136,137}} = \frac{135}{136} \cdot \frac{134 \cdot \delta\langle r^2\rangle^{134,135} - 136 \cdot \delta\langle r^2\rangle^{135,136}}{135 \cdot \delta\langle r^2\rangle^{135,136} - 137 \cdot \delta\langle r^2\rangle^{136,137}}. \quad (5)$$

The quantities η_i and κ_i were evaluated for all measured two-photon transitions i, as well as for the Ba I resonance line with the data given in [5]. The results are graphically presented in Fig. 4. Good agreement is found within the experimental errors, i.e. the nuclear parameters are independent of the electronic transition in which they are measured. For their weighted average we find $\eta = -1.423$ (10) and $\kappa = -1.123$ (13). An extraction of $\delta\langle r^2\rangle$ values from the data requires electronic information, e.g. $\Delta|\Psi(0)|^2$ must be known for the transitions investigated. Such information, however, is not available at present.

The financial support of the Deutsche Forschungsgemeinschaft is gratefully acknowledged. We wish to thank Dr. M. Wilson for valuable comments and discussions in the interpretation of the isotope shift results.

References

1. Rubbmark, J.R., Borgström, S.A., Bockasten, K.: J. Phys. B **10**, 421 (1977)
2. Aymar, M., Robaux, O.: J. Phys. B **12**, 531 (1979)
3. Jackson, D.A., Duong Hong Tuan: Proc. Roy. Soc. A **280**, 323 (1964)
4. Jackson, D.A., Duong Hong Tuan: Proc. Roy. Soc. A **291**, 9 (1966)
5. Nowicki, G., Bekk, K., Göring, S., Hanser, A., Rebel, H., Schatz, G.: Phys. Rev. C **18**, 2369 (1978)
6. Baird, P.E.G., Brambley, R.J., Burnett, K., Stacey, D.N., Warrington, D.M., Woodgate, G.K.: Proc. Roy. Soc. A **365**, 567 (1979)
7. Becker, W., Fischer, W., Hühnermann, H.: Z. Physik **216**, 142 (1968)
8. Fischer, W., Hartmann, M., Hühnermann, H.: Z. Physik **267**, 209 (1974)
9. Höhle, C., Hühnermann, H., Meier, Th., Wagner, H.: Z. Physik A **284**, 261 (1978)
10. Alvarez, E., Arnesen, A., Bengston, A., Hallin, R., Niburg, M., Nordling, C., Noreland, T.: Physica Scripta **18**, 54 (1978)
11. Heilig, K., Steudel, A.: Atomic Data and Nuclear Data Tables **14**, 613 (1974)
12. Vasilenko, L.S., Chebotayev, V.P., Shishaev, A.V.: JETP Lett. **12**, 113 (1970)
13. Cagnac, B., Grynberg, G., Biraben, F.: J. de Physique **34**, 845 (1973)
14. Hänsch, T.W., Harvey, K.C., Meisel, G., Schawlow, A.L.: Opt. Commun. **11**, 50 (1974)
15. Kopfermann, H.: Nuclear Moments, New York: Academic Press 1958
16. Moore, C.E.: Atomic Energy Levels III. (Circular 467), Washington DC: NBS (1971)
17. zu Putlitz, G.: Ann. Phys. **11**, 248 (1963)
18. Miles, B.M., Wiese, W.L.: Atomic Data **1**, 1 (1969)
19. Childs, W.J.: Case Studies in Atomic Physics **3**, 215 (1972)
20. Friedrich, H., Trefftz, E.: J. Quant. Spectrosc. Radiat. Transfer **9**, 333 (1969)
21. Rose, S.J., Pyper, N.C., Grant, I.P.: J. Phys. B **11**, 755 (1978)
22. Bauche, J., Champeau, R.-J.: Adv. Atom. Molec. Phys. **12**, 39 (1976)
23. King, W.H.: J. Opt. Soc. Am. **53**, 638 (1963)
24. King, W.H.: J. Phys. B **4**, 288 (1971)
25. King, W.H.: private communication

W. Jitschin
G. Meisel
Institut für Angewandte Physik
Universität Bonn
Wegelerstraße 8
D-5300 Bonn 1
Federal Republic of Germany